IEPC-2007-172

Ion Velocity Measurements within the Acceleration Channel of a Low Power Hall Thruster

William A. Hargus, Jr.
Air Force Research Laboratory
Edwards AFB, CA 93524

Michael R. Nakles
E.R.C., Inc.
Edwards AFB, CA 93524

Abstract

This work presents axial ion velocity measurements within the acceleration channel of the Busek Co. Inc. BHT-200 200 W laboratory Hall thruster derived from laser-induced fluorescence measurements of the $5d[4]_{7/2}$-$6p[3]_{5/2}$ xenon ion excited state transition. Acceleration channel centerline ion velocities were measured for one nominal and six related cases. These six cases were chosen to be representative of small variations of the applied propellant flow, magnetic field, and discharge charge potential from the nominal condition. These deviations in operating parameters translate into changes in the plasma density, electron transport, and applied electric field, respectively. The effect of varying the magnetic field, hence influencing the electron transport, is to adjust the location the internal ion acceleration. Increasing the anode propellant flow, which proportionally increases the plasma density and also influences the electron transport, appears to shift the acceleration upstream. Increasing discharge potential increases ion acceleration proportionally. Preliminary examination of the fluorescence traces, which have been previously shown to be representative of the ion velocity distributions, are also undertaken. From these data, it is possible to estimate internal axial electric fields and identify regions of ion acceleration and creation.

Introduction

The goal of this study is to characterize the xenon ion velocities inside the acceleration channel of a low power xenon Hall thruster using laser-induced fluorescence (LIF). These measurements are valuable for their use in the validation of device models of this and other various Hall thrusters. Previous internal measurements of ion velocities have been carried out using a slot cut into the side of a Hall thrusters [1] . These slots presumably affect the operation of the thruster. Even if the global effect is small, the local effect may be significant. Furthermore, slicing slots into Hall thruster side walls is not always possible with expensive, one of kind, test articles.

Most modern Hall thrusters have acceleration channels with a maximum depth of 1-2 cm. Therefore, it is possible to align collection optics to the probe beam such that limited internal optical access is possible without modification of the Hall thruster. In this work, the collection lens is placed 60° off the thrust axis. This minimizes plume impact since typically greater than 95% of a Hall thruster plume ion flux is contained in a 45° half angle. In this way, it is possible to completely non-intrusively probe internal ion acceleration of any modern Hall thruster.

Acceleration channel centerline ion velocities were measured for one nominal and six closely related additional cases. These six cases were chosen to be representative of small deviations of the applied propellant flow, magnetic field, and anode discharge potential from the nominal condition. These small parameter changes approximately translate into changes in the plasma density, electron transport, and applied electric field, respectively. The goal of this paper is to provide a preliminary survey of the effect on the ion acceleration profile produced by small operating parameter changes.

Previous attempts to compare bulk ion velocities from experiments with results of numerical simulations have encountered difficulties. For example, simulation efforts usually report mean velocities. Experimental methods such LIF are often noise limited and are better suited to determining the most probable velocity. In the skewed, non-symmetric velocity distributions common to Hall thrusters, the most probable (i.e. peak signal) and statistical mean velocities often differ. Ideally, comparison of the velocity distribution function determined from each method would minimize ambiguity. Fluorescence traces have been previously shown to be representative of the ion velocity distribution function (VDF) [2]. This study therefore includes a preliminary effort to extract and present these data.

Xenon Laser Induced Fluorescence

LIF is a convenient diagnostic for the investigation of ion and atomic velocities as it does not perturb the plasma. The LIF signal is a convolution of the VDF, transition line shape, and laser beam frequency profile. Determination of the VDF from LIF data only requires the deconvolution the transition line shape and laser beam profile from the raw LIF signal trace.

For the results reported here, the $5d[4]_{7/2}$-$6p[3]_{5/2}$ electronic transition of Xe II at 834.7 nm is probed. The isotopic and nuclear-spin effects contributing to the hyperfine structure of the $5d[4]_{7/2}$-$6p[3]_{5/2}$ xenon ion transition produce a total of 19 isotopic and spin split components. The hyperfine splitting constants which characterize the variations in state energies are only known for a limited set of energy levels. Unfortunately, the 834.7 nm xenon ion transition only has confirmed data on the nuclear spin splitting constants of the $6p[3]_{5/2}$ upper state [1,3-5]. Manzella and others have previously used the $5d[4]_{7/2}$-$6p[3]_{5/2}$ xenon ion transition at 834.7 nm to make velocity measurements in a Hall thruster plume [1-2,6-8]. A convenient feature of this transition is the presence of a relatively strong line originating from the same upper state ($6s[2]_{3/2}$-$6p[3]_{5/2}$ transition at 541.9 nm [9] which allows for non-resonant fluorescence collection.

Ion velocity is determined by measurement of the Doppler shift of the absorbing ions. If an absorber has a velocity component $\boldsymbol{u}$ along the axis of the laser beam, it will absorb the light at a frequency shifted from that of stationary absorbers. The magnitude of this frequency shift $\partial\boldsymbol{\nu}_{12}$ depends on the speed $\boldsymbol{u}$ along the laser beam axis

$$\partial\nu_{12} = \nu_{12}\frac{u}{c} \qquad [1]$$

where $\boldsymbol{c}$ is the speed of light. The Doppler shift of a species' fluorescence profile away from the line center $\boldsymbol{\nu}_{12}$ of stationary absorbers is in proportion to $\boldsymbol{u}$ [10].

Previous measurements and analysis have shown that deconvolution is not strictly required to estimate xenon ion VDFs from the raw LIF data in this plasma discharge for this particular xenon transition [2]. The VDF near the exit plane is sufficiently broad that is does not require deconvolution of the transition line shape. Not performing the deconvolution further in the plume (e.g. beyond the cathode plane) may introduce uncertainties estimated to be less than 20%.

Experimental Apparatus

The measurements in this effort were performed in Chamber 6 of the Air Force Research Laboratory (AFRL) Electric Propulsion Laboratory at Edwards AFB, CA. Chamber 6 is a non-magnetic stainless steel chamber with a 1.8 m diameter and 3 m length. It has a measured pumping speed of 32,000 l/s on xenon. Pumping is provided by four single stage cryogenic panels (single stage cold heads at ~25 K) and one 50 cm two stage cryogenic pump (<12 K). Chamber pressure during thruster operation is approximately $7\text{x}10^{-4}$ Pa, corrected for xenon.

The Hall thruster used in this study is the Busek Company BHT-200 200 W Hall thruster which has been described elsewhere [11]. Table 1 shows the nominal operating conditions for the BHT-200 thruster during this test. During thruster operation, the parameters shown in Table 1 are monitored and recorded at a 0.2 Hz data rate.

Table 1. Nominal Thruster Operating Conditions

Anode Flow	840 µg/s (Xe)
Cathode Flow	98 µg/s (Xe)
Anode Potential	250 V
Anode Current	0.75 A
Keeper Current	0.5 A
Magnet Current	1.0 A
Heater Current	3.0 A

The thruster is mounted on a three axis orthogonal computer controlled translation system. Figure 1 shows the Hall thruster and optics mounted within the vacuum chamber as well as the LIF apparatus. The laser is a New Focus Vortex tunable diode laser. It is capable of tuning approximately ±50 GHz about a center wavelength of 834.7 nm. The 6 mW beam is passed through a Faraday isolator to eliminate feedback to the laser. The laser beam then passes through several beam pick-offs until it is focused by a lens and enters the vacuum chamber through a window. The probe beam is chopped at a frequency by an optical chopper (Ch2 at 2.8 kHz) for phase sensitive detection of the fluorescence signal.

The two wedge beam pick-offs (/BS) shown in Fig. 1 provide portions of the beam for diagnostic purposes. The first beam pick-off directs a beam to a photodiode detector (D1) used to provide constant power feedback to the laser. The second beam is divided into two equal components by a 50-50 cube beam splitter. The first component is directed to an Burleigh WA-1500 wavemeter used to monitor absolute wavelength. The second component is sent through an optical chopper (Ch1 at 1.4 kHz) and through a low pressure xenon hollow cathode discharge lamp. The lamp provides a stationary absorption reference for the determination of the Doppler shift $\partial\boldsymbol{\nu}_{12}$. Unfortunately, there is no detectable population of the ionic xenon $5d[4]_{7/2}$ state. However, there is a nearby (18.1 GHz distant) neutral xenon $6s'[1/2]_1$-$6p'[3/2]_2$ transition at 834.68 nm [12-13]. The second pick-off sends a beam to a 300 MHz free spectral range Fabry-Perot etalon (F-P) that provides high resolution frequency monitoring of the wavelength interval swept during a laser scan.

The fluorescence collection optics are also shown in Fig. 1. The fluorescence is collected by a 75 mm diameter, 300 mm

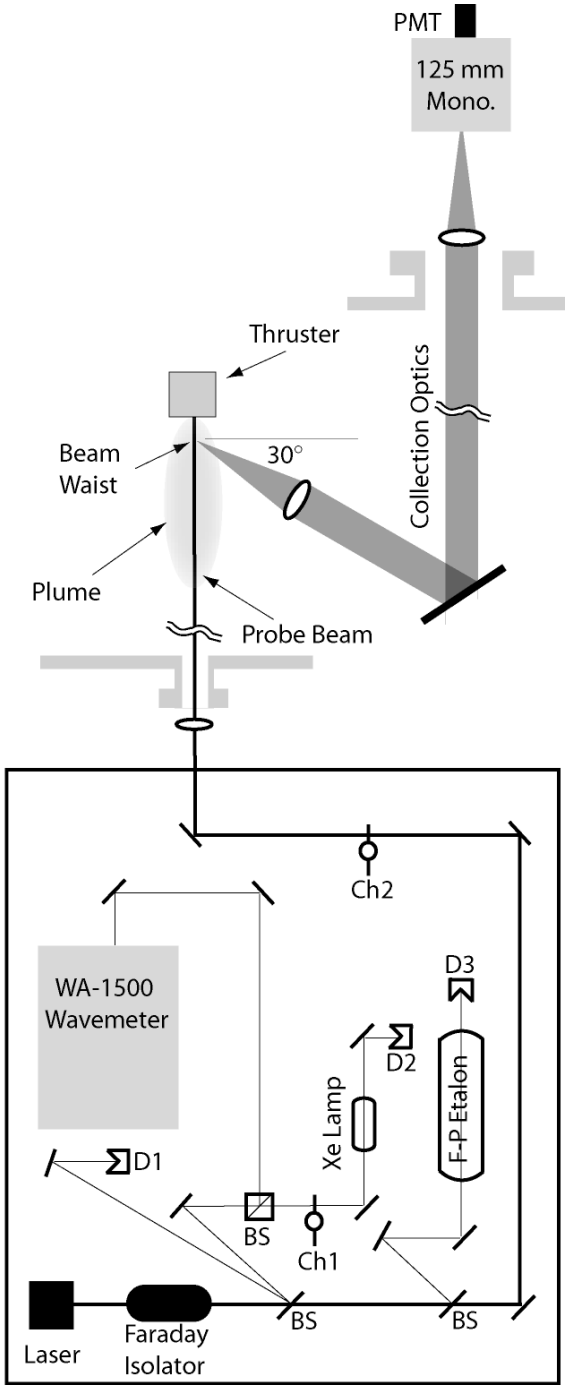

Fig. 1. Top view diagram of the laser optical train and collection optics.

focal length lens within the chamber and oriented 60° from the probe beam axis. The collimated fluorescence signal is directed through a window in the chamber side wall to a similar lens that focuses the collected fluorescence onto the entrance slit of 125 mm focal length monochrometer with a photomultiplier tube (PMT). Due to the 1:1 magnification of the collection optics, the spatial resolution of the measurements is determined by the geometry of the entrance slit 0.7 mm width and 1.5 mm height as well as the sub-mm diameter of the probe beam. This

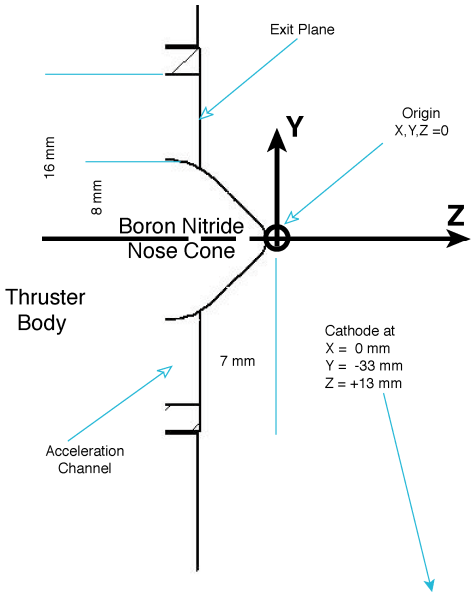

Fig. 2. Near field dimensions of the BHT-200 Hall thruster with origin of the coordinate system and positions of critical dimensions and locations noted.

apparatus allows for limited probing of the interior acceleration channel of Hall thrusters with relatively shallow acceleration channels.

Figure 2 shows the near field geometry of the Busek BHT-200 Hall thruster. The locations of the protruding central magnetic pole (nose cone) and edges of the acceleration channel are indicated as is the position of the cathode exit. The cartesian coordinate system and origin used in these measurements is also shown. The coordinate system orientation is also referenced in Figs. 1 and 2. The origin is 0.5 mm beyond the tip of the nose cone due to the repeatability with which this position may be located. All locations are referenced to these coordinates. Measurements presented in this work will be limited to the Y = 12 mm, X = 0 mm line and do not generally extend beyond the tip of the nose cone.

Results and Discussion

Understanding and characterizing the internal ion acceleration is highly important for understanding the fundamental mechanisms governing of Hall thruster operation. Furthermore, from these velocity profiles, one may extract estimates of the electric field. LIF allows this to be done without the introduction of any disturbing foreign object, such as an electro-static probe. Previous measurements have shown that the introduction of probes into the acceleration channel appears to move the apparent acceleration zone upstream, further into the thruster than what is indicated by LIF measurements [1].

It has been shown previously that the xenon ions emitted from a Hall thruster undergo considerable acceleration between the thruster's physical exit plane and cathode plane [1-2,14]. The ion flow evolves in the near plume region and the thruster

cannot be fully characterized without recognizing the external acceleration. This effort examines the external ion acceleration to a distance of 7 mm beyond the exit plane, equal to the distance from the exit plane to the tip of the boron nitride nose cone.

Test results will be presented in four sections. The first section will discuss data taken at the nominal thruster operating condition as specified in Table 1. The second section will describe the results of varying the magnetic field on the ion velocity profile. The third section will describe the effects on the velocity profiles due to changes in the anode propellant flow. The fourth section will examine the effect of varying the applied anode discharge potential. The velocities presented in the first four sections are based on the use of single velocities taken from the LIF measured distributions and correspond to the most probable velocity. These velocities can be identified with the least uncertainty and greatest repeatability. Finally, the fifth section will analyze the VDF data gleaned from the fluorescence traces for the nominal thruster condition. In each data set, the goal is to determine the effect of isolated, small operating parameter variations on the ion acceleration process. In all cases, data is only taken in the acceleration channel center at X = 0 mm and Y= 12 mm. Values for the axial (Z) position typically varied from 0 to -13 mm.

In all cases, the most probable velocities are within an uncertainty of ±500 m/s, or better. The repeatability of the trace peaks appears to be a fraction of the quoted uncertainty (±80 m/s). However, the fluorescence line shapes are often significantly broadened, due to wide velocity distributions. The quoted uncertainty should therefore be viewed as the uncertainty in the determination of the peak of the fluorescence line shape. This peak represents the most probable ion velocity. It should also be noted that there also exists some uncertainty in the precise separation between the ion and neutral transitions, and this also represents another potential source of measurement uncertainty.

Nominal Case

The conditions for the nominal case are shown in Table 1. Figure 3 shows the most probable ion velocity evolution from Z = -13 mm to Z = 2 mm. The ion velocity climbs from 500 m/s at Z = -13 mm, to 12.6 km/s at the exit plane. The ion velocity continues to increase beyond the thruster exit to until the limit of the measurement space (Z = 2 mm) where the velocity increases to 16.2 km/s. From these velocity measurements, it is possible to calculate ion kinetic energies which may then be differentiated to approximate the effective electric field acting on the flow of ions.

Figure 4 shows both the calculated ion energies and the derived electric field. The ion energy data show that only 108 eV of the 250 V applied potential are recovered by the propellant within the thruster interior. An additional 66 eV are recovered by Z = 0, and a further 4 eV are recovered 2 mm downstream. This is reflected in the derived electric field which shows a peak at Z = -9 mm, 2 mm into the thruster, and a gradual decay outside the thruster consistent with measured external ion acceleration.

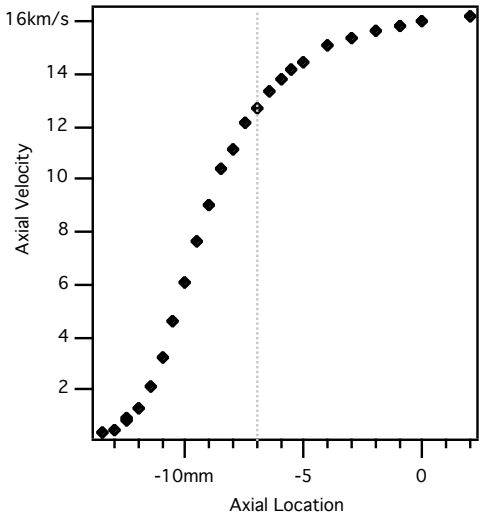

Fig. 3. Nominal case ion velocity profile. Thruster exit denoted by line at Z = -7 mm.

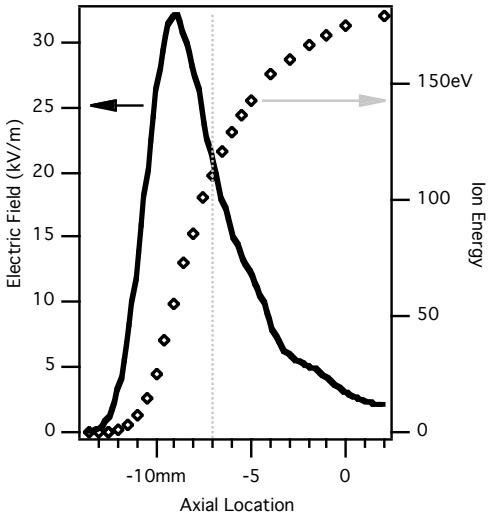

Fig. 4. Nominal case ion energy profile with derived electric field. Thruster exit plane is denoted by line at Z = -7 mm.

Variation of Magnetic Field

In a Hall thruster, the purpose of the magnetic field is to magnetize the electrons to retard their progress toward the anode and thereby produce an electric field to accelerate the ions which are produced by electron impact. It is therefore informative to examine the effect of magnetic field on the ion velocity profile and hence the internal electric field. Figure 5 shows the ion velocities in the measurement range for the nominal case and a case with approximately 25% reduction in the magnetic field. The final velocities are the same at Z = 0; however, the ion acceleration is delayed by the lower magnetic field strength. The net result is that the electric field is higher for the reduced magnetic field case by nearly 20% as seen in Fig. 6. Interestingly, not only is the electric field is significantly higher than

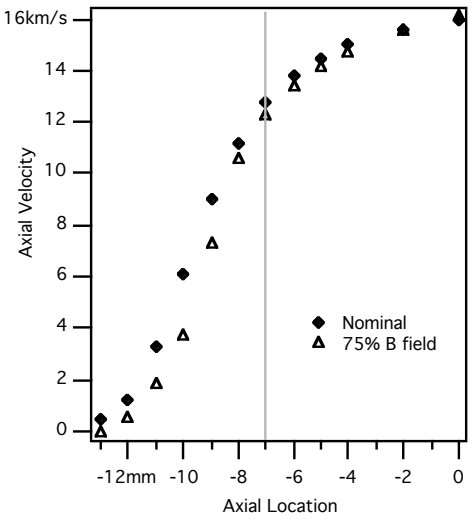

Fig. 5. Nominal case and reduced magnetic field case ion velocity profiles.

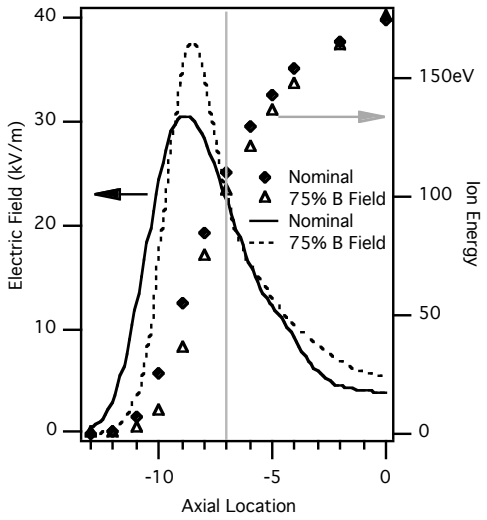

Fig. 6. Nominal case and reduced magnetic field case ion energy profiles and derived electric field.

the nominal case when the magnetic field is decreased 25%, but the location of the peak electric field moves downstream by approximately 0.5 mm. In this case, it appears that the optimal value for the magnetic field may in fact be closer to the lower value than it is to the nominal value, especially in the light of similar energy recovery and the more downstream acceleration of the reduced magnetic field case. However, the lower magnetic field strength case also exhibits increased external electric field which may be indicative of higher divergence losses.

A subsequent simulation of the static magnetic field has shown that the peak of the radial magnetic field peak also shifts downstream by slightly less than 1 mm from the nominal to the 25% reduced field strength case. These measurements appear to be able to accurately capture the results of very small shifts in thruster parameters.

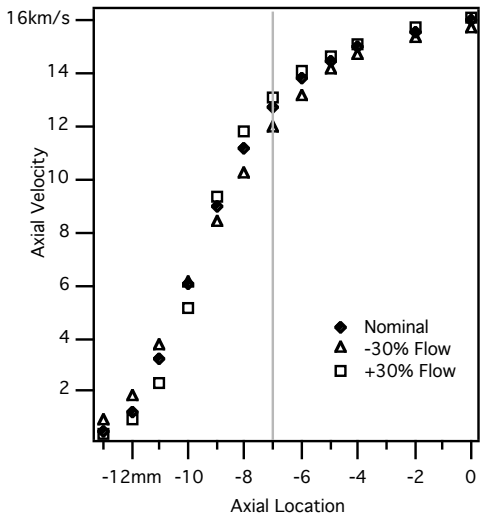

Fig. 7. Nominal ±30% anode flow cases ion velocity profiles.

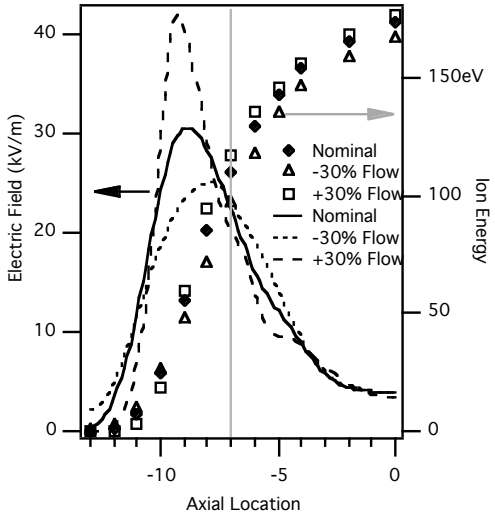

Fig. 8. Nominal and ±30% anode flow cases ion energy profiles and derived electric fields.

Variation of Anode Propellant Flow

Variation of the propellant flow to the anode discharge is a straightforward method to vary the plasma density within the thruster discharge. Since classical cross-field electron conductivity relies on electron collisions with heavy particles to provide pathways for electrons through the radial magnetic field, it can be assumed a priori that the electron conductivity will increase with anode flow resulting a more abrupt acceleration and hence a higher electric field. The result is similar to that seen in the previous case of reduced magnetic field.

Figures 7 and 8 show two cases in addition to the nominal case. These cases correspond to ±30% anode propellant flow from the nominal case. It is interesting to note that the effect of decreasing anode flow, does not allow for the same ion energy

recovery at Z = 0 mm. The nominal and +30% flow cases recover 174 and 177 eV, respectively; but the -30% flow case only recovers 167 eV at the same location. It is postulated that since the location of the peak electric field has been shifted closer to the thruster exit, the ion acceleration may be more prone to loss mechanisms such as divergence. Unlike the previous case of the reduced magnetic field, the increased flow case both increases electric field (33%) and and moves its peak upstream (~0.5 mm) when compared to the nominal case. The reduced flow case moves the electric field peak downstream by 1 mm and decreases its magnitude by 16%. This is consistent with previously observed behavior where neutral background pressure greatly affected the acceleration profiles in a thruster with predominantly external acceleration [15]. It may also fundamentally explain the increases in performance seen in vacuum facilities with high background pressures.

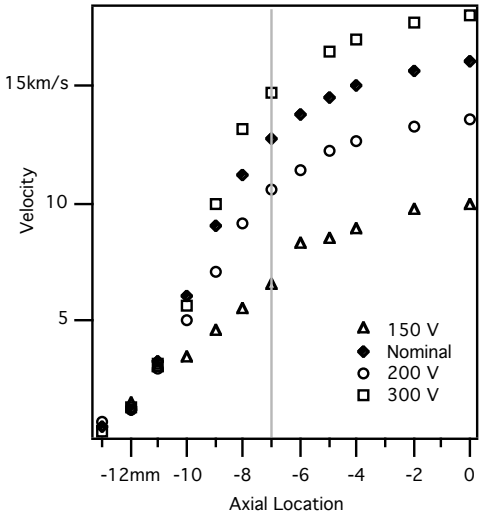

Fig. 9. Velocity profiles for varied discharge potentials; 150 V, 200V, 250 V (nominal), and 300 V.

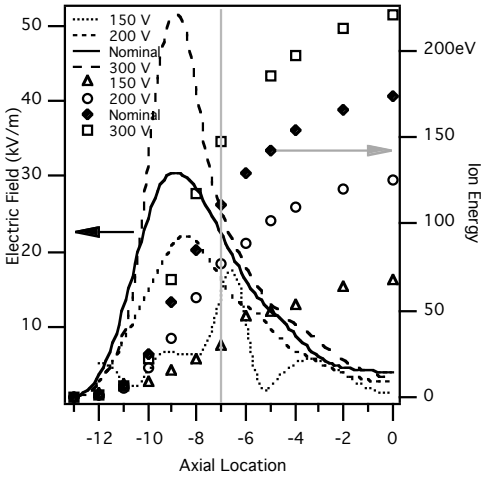

Fig. 10. Ion energy profiles and derived electric fields for varied discharge potentials; 150 V, 200V, 250 V (nominal), and 300 V.

Variation of Discharge Potential

Three cases of anode discharge potential were examined in addition to the nominal case of 250 V. These include anode potentials of 150 V, 200 V, and 300 V. In the simplest sense, varying the discharge potential should provide a clear method to vary the internal electric field. The velocity, ion energies, and derived electric fields are shown in Figs. 9 and 10.

As expected, the ion velocities and energies are a strong function of the applied discharge potential. Although the nominal cases peak is calculated to be slightly downstream of the 200 and 300 V cases (~0.2 mm), the peak of the derived electric field does not appear to vary in location appreciably. However, the electric field magnitude does change, but not linearly. A 20% increase in applied discharge potential (250 to 300 V) increases the peak field strength by 70%, while a 20% decrease (250 to 200 V) only decreases the peak electric field by 28%.

In Fig. 11, the calculated kinetic energies shown in Fig. 10 are normalized by the discharge potential less 60 V. The value of 60 V is taken from plume measurements 107 mm downstream of the exit plane where the ion energies appear to never exceed the the discharge potential minus 60 V [2,14]. Figure 11 shows that this normalization tightly groups the nominal case (250 V) with the 200 and 300 V cases, but the 150 V case lags by 20% in recovery of the applied discharge potential.

It is obvious that the 150 V case is very different from the

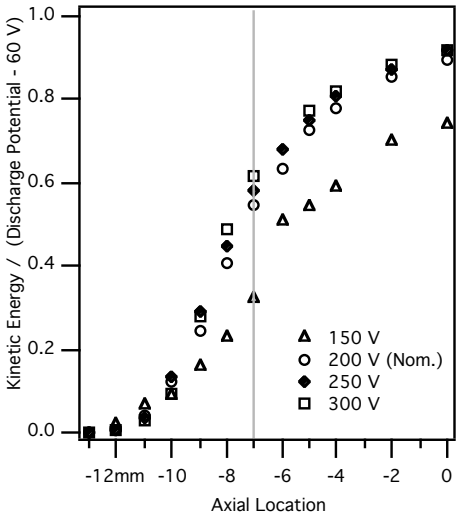

Fig. 11. Kinetic energies from Fig. 10 normalized by the thruster discharge potential minus 60 V.

other three cases. Not only is the velocity and proportional energy recovery lower than the other cases examined, but the raw LIF signal to noise ratio (SNR) was also very poor. This decreased SNR appears to be the result of increased plasma oscillations in the measurement region which were close to the phase frequency of the lockin amplifier. It is therefore obvious that this case is large departure from the nominal condition as is aptly illustrated in Figs. 10 and 11.

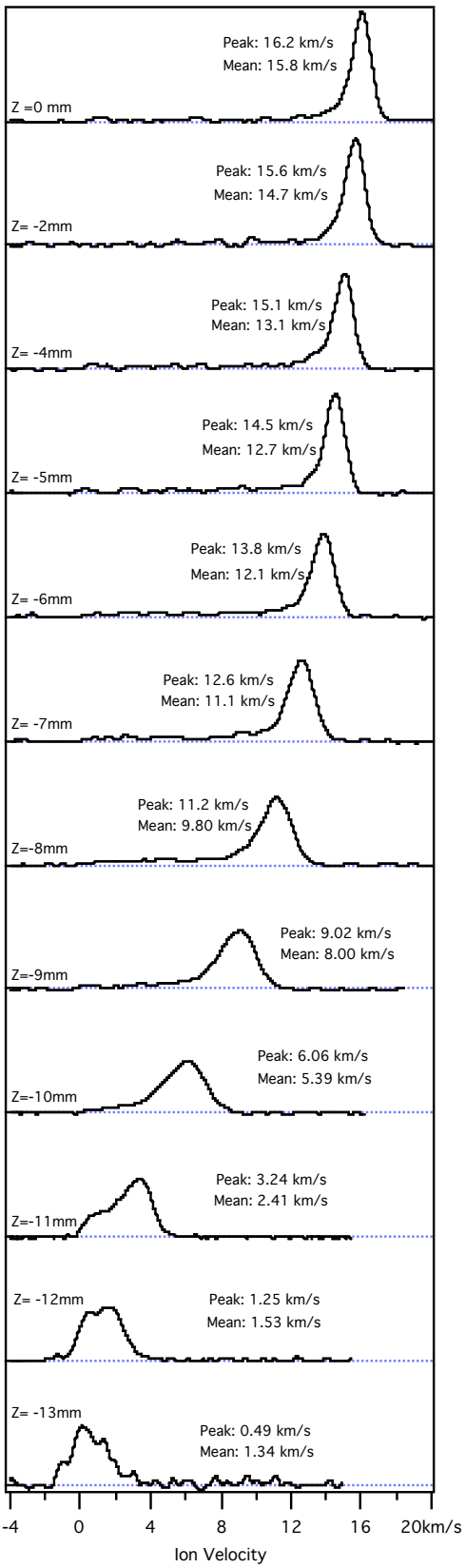

Fig. 12. Nominal case ion velocity distributions from LIF traces. Each distribution is area normalized.

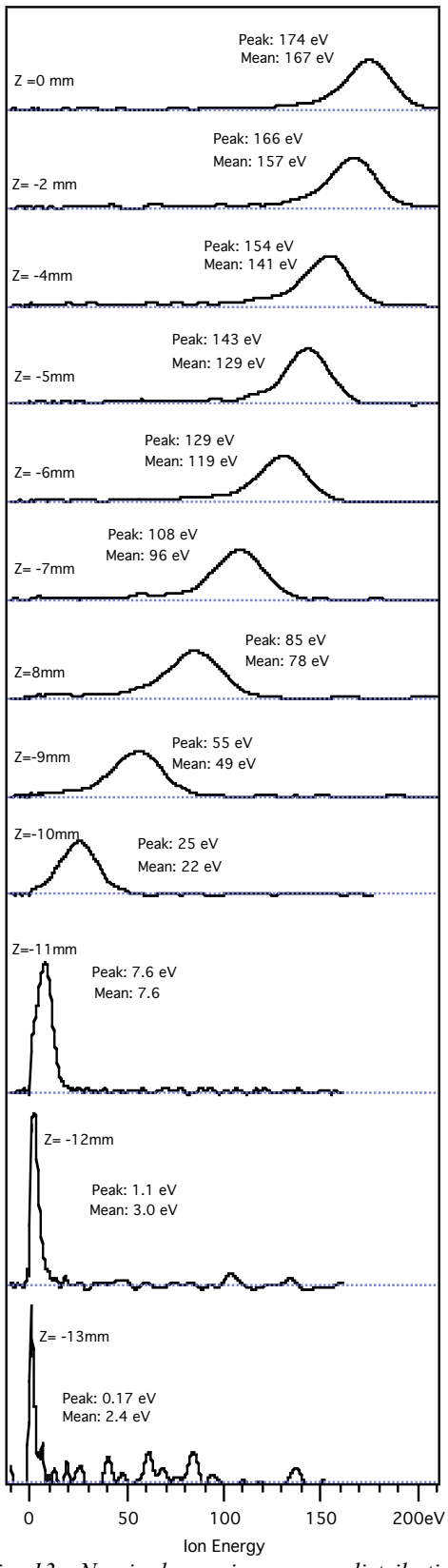

Fig. 13. Nominal case ion energy distributions derived from LIF traces. Each distribution is area normalized.

Velocity Distributions

The previous results and discussion are based on the use of single velocities taken from the LIF measured distributions and correspond to the most probable velocity. Laser-induced fluorescence (LIF) traces are very often noisy and the most probable velocity can be determined with minimum uncertainty. In the skewed, non-symmetric velocity distributions common to Hall thrusters, the most probable (e.g. peak signal) and statistical mean velocities may differ. Fluorescence traces have been previously shown to be representative of the ion velocity distribution function [2]. This is especially true in the very near field of the Hall thruster where the broad fluorescence trace does not require deconvolution of the relatively narrow $5d[4]_{7/2}$-$6p[3]_{5/2}$ transition line shape.

The velocity distributions shown in Fig. 12 are from the nominal case as specified in Table 1. Here the ion acceleration evolves from Z = -13 mm through the exit plane (Z = -7 mm) to the final measurement at Z = 0 mm. The width of the VDF decreases as the bulk flow is accelerated through the potential fall within the the Hall thruster acceleration channel. However in nearly all cases, traces of a low velocity population is visible between 0 m/s and the peak velocity. This population may be the result of distributed ionization, possible due to ionization of previously recombined ions which were accommodated by the wall.

Further upstream as the VDF broadens significantly, there is evidence of multiple ion populations, particularly at Z = -11 and -12 mm. At Z = -12 mm, there appear to be two partially overlapped populations of ions; one nearly stationary and one with 3.24 km/s axial velocity. From this, it appears that a particularly active region of ionization occurs in this immediate region with only a relatively small amount of ionization occurring downstream. Although from the low velocity tail that apparent in most of the VDF data, it is apparent that some level of ionization continues throughout the entire ion acceleration.

Figure 13 contains energy distributions derived from the VDF data in Fig. 12. Furthest upstream, the ion energy distribution is a very narrow, sharp peak. The distribution remains so until Z = -10 mm where the ions first begin appreciable acceleration (25 eV or 6 km/s). The shapes of the energy distributions reinforce the supposition that the primary region of ionization is at or upstream of Z = -11 mm. This may account for much lower signal levels upstream of this point [11].

Although the extraction of VDF data from LIF data has been previously demonstrated for this transition [2], the derivation of energy distributions is more prone to uncertainties due to the multiplicative nature of the calculation. This becomes increasingly important at high velocities where even a small amount of broadening in the VDF can greatly affect the shape of the derived energy distribution. As such, the energy distributions should be viewed as a limited quantitative tool, but useful in understanding the acceleration behavior of the plasma. Figures 12 and 13 also are annotated with the peak and mean velocities and energies for each transition. The peak values are for the most part unambiguous; however, the calculation of the mean values introduces greater uncertainty primarily due to noise in the signal baseline. This is especially true for the low velocity tail that is evident in nearly all the distributions.

Conclusions

This effort has non-intrusively measured xenon ion velocity profiles in the center of the acceleration channel of a low power (200 W) Hall thruster for one nominal condition and 6 additional conditions which deviated from the nominal condition by the variation of only one control factor (i.e. magnetic field strength, propellant flow, and discharge potential). From these velocity profiles energy deposition and effective electric fields were calculated. In addition, the velocity distributions taken from the LIF data are presented for the nominal case. This appears to be the first effort to measure internal ion velocity data within an unmodified Hall thruster and is as such a completely non-intrusive spatially resolved internal measurement of internal plasma parameters.

From the measurements, several generalizations can be made for this Hall thruster. Lowering the magnetic field strength pushes the acceleration region downstream in close correspondence with the shift in the peak magnetic field. Reducing the magnetic field strength resulted in nearly identical utilization of the applied potential as the nominal case. This occurs due to an increase in the internal electric field which for a 25% decrease in field strength yields a 20% increase in peak electric field as well as elevated external field strength.

Varying the anode flow, and hence the plasma density, shifts the velocity profiles significantly. Increasing the propellant flow both moves the peak electric field upstream and increases the magnitude. In the cases examined, a flow increase of 30% increased the electric field by 33%; while a similar decrease reduced the electric field by 16%. In addition, the energy recovery of the nominal and higher flow cases appeared to be higher than the lowest flow case, perhaps due to the shift downstream of the peak electric field. It is also interesting to note that several unpublished near field LIF studies of this thruster have shown a similar trend when comparing the nominal velocity profiles for vacuum facility base and elevated background pressures. It observed that increases in the background pressure (4x) increased the exit velocity by 5-8%. These increases remained until (and presumably beyond) 107 mm from the exit plane, the limit of the measurement region. These two results hint that the question of understanding Hall thruster performance measurements at elevated background pressures is significantly more complex than the simple ingestion of background neutral atoms [16].

The interpretation of Hall thruster velocity profiles for varied anode potentials appears more straightforward with increases in discharge potential increasing the peak electric field. For most of the cases examined, the fraction of energy recovered appear to approximate the discharge potential less 60 V. There are also some interesting differences. For example, increasing discharge potential sharpens the electric field peak changing its shape. While lowering the discharge potential produces a field geometrically similar to the nominal case but with a lower magnitude. Lowering the discharge potential substantially appears to have drastically reduced the energy recov-

ery and produced a significantly lower magnitude and shaped electric field profile.

The VDF and energy distribution data for the nominal case provide an indication of the primary ionization region and also provide clear evidence that ionization continues, albeit at lower rates, throughout the flow field. Future analysis will examine similar data for the 6 other operating conditions. These will allow a greater pinpointing of the differences between these operating conditions. It also anticipated that these data will be used for comparison and validation of numerical models.

Acknowledgments

The authors would like to gratefully acknowledge the assistance of Garrett Reed in the development of the LIF data acquisition system as well as Lubos Brieda for his discussions of numerical Hall thruster modeling and their comparison to experimental data.

References

1. W. A. Hargus, Jr. and M. A. Cappelli, "Laser-Induced Fluorescence Measurements of Velocity within a Hall Discharge," *Applied Physics B,* Vol. 72, pp 961-969, 2001.

2. W. A. Hargus, Jr. and M. R. Nakles, "Evolution of the Ion Velocity Distribution in the Near Field of the BHT-200-X3 Hall Thruster," AIAA-2006-4991, *42nd Joint Propulsion Conference,* 9-12 July 2006, Sacramento, CA.

3. H. Geisen, T. Krumpelmann, D. Neuschafer, and Ch. Ottinger, "Hyperfine Splitting Measurements on the 6265 Å and 6507 Å Lines of Seven Xe Isotopes by LIF on a Beam of Metastable Xe(3P0,3) Atoms," *Physics Letters A,* Vol. 130, No. 4.5, 11 July, 1988.

4. W. Fischer, H. Huhnermann, G. Kromer, and H.J. Schafer, "Isotope Shifts in the Atomic Spectrum of Xenon and Nuclear Deformation Effects," *Z. Physik,* Vol. 270, No. 113, 1974.

5. L. Bronstrom, A. Kastberg, J. Lidberg, S. Mannervik, "Hyperfine-structure Measurements in Xe II," *Physical Review A,* Vol. 35, No. 1, Jan. 1996.

6. D. H. Manzella, "Stationary Plasma Thruster Ion Velocity Distribution," AIAA-94-3141, *30th Joint Propulsion Conference,* 27-29 June 1994, Indianapolis, IN.

7. J. E. Pollard and E. J. Beiting, "Ion Energy, Ion Velocity, And Thrust Vector Measurements For The SPT-140 Hall Thruster," *3rd International Conference on Spacecraft Propulsion,* 10-13 Oct. 2000, Cannes, France.

8. T. E. Smith, B. B. Ngom, J.A. Linnell, A.D Gallimore, "Diode Laser-Induced Fluorescence of Xenon Ion Velocity Distributions," AIAA-2005-4406, *41st Joint Propulsion Conference,* 11-13 July 2005, Tucson, AZ.

9. J. E. Hansen and W. Persson, "Revised Analysis of Singly Ionized Xenon, Xe II," *Physica Scripta,* Vol. 36, pp 602-643, 1987.

10. W. Demtroder, *Laser Spectroscopy: Basic Concepts and Instrumentation,* Springer-Verlag, Berlin, 1996

11. V. Hruby, J. Monheiser, B. Pote, P. Rostler, J. Kolencik, and C. Freeman, "Development of Low Power Hall Thrusters," AIAA-1999-3534, *30th Plasma Dynamics and Lasers Conference,* 28 June -1 July 1999, Norfolk, VA.

12. M. H. Miller and R. A. Roig, "Transition Probabilities of Xe I and Xe II," *Physical Review A,* Vol. 8, pp 480-486, July 1973.

13. C. E. Moore, *Atomic Energy Levels: Volume II,* Washington: National Bureau of Standards, pp 113-123, 1958.

14. W. A. Hargus, Jr. and C. S. Charles, "Near Exit Plane Velocity Field of a 200 W Hall Thruster," AIAA-2003-5154, *39th Joint Propulsion Conference,* 20-23 July 2003, Huntsville, AL.

15. N. Gascon, M. A. Cappelli, and W. A. Hargus, Jr., "Ion Velocity Measurements in a Linear Hall Thruster," AIAA-2005-4401, *41st Joint Propulsion Conference,* 10-13 July 2005, Tucson, AZ.

16. T. Randolph, V. Kim, H. Kaufman, K. Korzubusky, V. Zhurin, and M. Day, "Facility Effects on Stationary Plasma Thruster Testing," IEPC-1993-093, *23rd International Electric Propulsion Conference,* 23-27 Sept. 1993, Seattle, WA.